THE JOURNAL OF BIOLOGICAL CHEMISTRY VOL. 287, NO. 3, pp. 1970–1979, January 13, 2012

Dual Beneficial Effect of Interloop Disulfide Bond for Single Domain Antibody Fragments*[S]

Received for publication, March 23, 2011, and in revised form, November 21, 2011 Published, JBC Papers in Press, November 29, 2011, DOI 10.1074/jbc.M111.242818

Jochen Govaert[1,2], **Mireille Pellis**[1,2], **Nick Deschacht**[2], **Cécile Vincke**, **Katja Conrath**[3], **Serge Muyldermans**[4], **and Dirk Saerens**

From the Laboratory of Cellular and Molecular Immunology, Vrije Universiteit Brussel, Pleinlaan 2, B-1050 Brussels, Belgium and the Department of Structural Biology, Vlaams Interuniversitair Instituut voor Biotechnoloogie (VIB), Pleinlaan 2, B-1050 Brussels, Belgium

Background: The presence of cystines connecting antigen-binding loops in single domain antibodies is puzzling.
Results: Cysteines forming such cystine are substituted, and the performance of functional antibody fragments is determined.
Conclusion: An interloop disulfide bond stabilizes the domain and rigidifies the long third antigen-binding loop, leading to stronger antigen interaction.
Significance: This beneficial effect explains *in vivo* antibody maturation favoring antibodies with an interloop disulfide bond.

The antigen-binding fragment of functional heavy chain antibodies (HCAbs) in camelids comprises a single domain, named the variable domain of heavy chain of HCAbs (VHH). The VHH harbors remarkable amino acid substitutions in the framework region-2 to generate an antigen-binding domain that functions in the absence of a light chain partner. The substitutions provide a more hydrophilic, hence more soluble, character to the VHH but decrease the intrinsic stability of the domain. Here we investigate the functional role of an additional hallmark of dromedary VHHs, *i.e.* the extra disulfide bond between the first and third antigen-binding loops. After substituting the cysteines forming this interloop cystine by all 20 amino acids, we selected and characterized several VHHs that retain antigen binding capacity. Although VHH domains can function in the absence of an interloop disulfide bond, we demonstrate that its presence constitutes a net advantage. First, the disulfide bond stabilizes the domain and counteracts the destabilization by the framework region-2 hallmark amino acids. Second, the disulfide bond rigidifies the long third antigen-binding loop, leading to a stronger antigen interaction. This dual beneficial effect explains the *in vivo* antibody maturation process favoring VHH domains with an interloop disulfide bond.

Antibodies, which play a crucial role in the adaptive immune system, are members of the immunoglobulin protein superfamily (1). The polypeptide sequences of the heavy chain and the light chain are compacted in several immunoglobulin domains. These antibody domains are folded in two β-sheets comprising either 5 + 4 or 3 + 4 antiparallel β-strands for the variable or constant immunoglobulin domains, respectively (2) (the β-strands are named A through G for the constant domain with variable domains having extra strands C′ and C″). An important hallmark of the immunoglobulin fold is the conserved disulfide bond located between cysteines of β-strands B and F at amino acid positions 23 and 104 (ImMunoGeneTics numbering (3); see Fig. 1). The importance of this conserved cystine in the folding and intrinsic stability of the immunoglobulin domain is well established. Its presence constrains the unfolded protein and thus reduces mainly the entropy of the unfolded state (4–8). The ability of an intradomain disulfide bond to increase the domain stability and subsequently the functionality has fueled research into rational design of cystines into proteins. Unfortunately, engineering disulfide bonds into proteins does not always increase stability because formation of a disulfide bond in the folded protein may displace the surrounding amino acids toward a less favorable position (5, 9). The lack of consistent rules to select appropriate loci for the introduction of disulfide cross-links hampers the rational design of stabilized proteins.

Until 1993, functional antibodies were always considered to comprise two identical heavy chains and two identical light chains. This view changed with the discovery of functional heavy chain antibodies (HCAbs)[5] lacking light chains in Camelidae (*i.e. Camelus dromedarius*, *Camelus bactrianus*, *Lama glama*, *Lama guanicoe*, *Lama pacos*, and *Lama vicugna*) (10). The immunoglobulin domain corresponding to the first constant domain in the heavy chain of classic antibodies, *i.e.* the CH1, is missing in the heavy chain of HCAbs. Hence, the antigen-binding fragment of a classic antibody, *i.e.* the Fab, is reduced to a single variable immu-

* This work was supported in part by the VIB, Fonds voor wetenschappelijk onderzoek-Vlaanderen (FWO-Vlaanderen), and Vrije Universiteit Brussel (Onderzoeksraad and Geconcerteerde Onderzoeks Acties).
[S] This article contains supplemental Fig. S1.
[1] Both authors contributed equally to this work.
[2] Supported by the Instituut voor de aanmoediging van Innovatie door Wetenschap en Technologie in Vlaanderen (IWT-Vlaanderen).
[3] Present address: Galapagos NV, Generaal De Wittelaan L11 A3, B-2800 Mechelen, Belgium.
[4] To whom correspondence should be addressed: Laboratory of Cellular and Molecular Immunology, VIB Dept. of Structural Biology, Vrije Universiteit Brussel, Pleinlaan 2, B-1050 Brussels, Belgium. Tel.: 32-2-629-19-69; Fax: 32-2-629-19-81; E-mail: svmuylde@vub.ac.be.

[5] The abbreviations used are: HCAb, heavy chain antibody; VHH, variable domain of heavy chain of HCAbs; FR-2, framework region-2; VL, variable light chain domain; VH, variable domain of a heavy chain; CDR, complementarity-determining region; B2H, bacterial two hybrid; HEWL, hen egg white lysozyme; RaPID, rate plane with isoaffinity diagonals; GdmCl, guanidinium chloride; PSA, prostate-specific antigen.

noglobulin domain in the HCAb. This variable domain referred to as variable domain of heavy chain of HCAbs (VHH) is adapted to become functional in antigen binding in the absence of a variable light chain domain (VL). As such, the VHH contains in its framework region-2 (FR-2), the region that in the variable domain of a heavy chain (VH) of a classic antibody interacts intimately with the VL, a number of hallmark amino acid substitutions that render the isolated domain more hydrophilic and more soluble than an isolated VH domain (10) (see Fig. 1). It has been demonstrated repeatedly that the VHH, cloned and expressed in bacteria, is a strict monomeric, single domain antigen-binding entity (11). It was noticed immediately that many VHHs of dromedary HCAbs possess an additional disulfide bond between the complementarity-determining region-1 (CDR1) and CDR3 loops (12). The Cys in the CDR1 is encoded in the *VHH* germ line genes (13), and this points toward a possible functional role of the interloop disulfide bond as an evolutionary pathway for domain and CDR loop stabilization.

Evidence supporting the stabilizing role of a disulfide bond to rigidify the CDR loops also came from the variable domains of platypus (14) and shark antibodies (15, 16), which possess an analogous interloop cystine. Finally, the selection of an interloop disulfide in a fibronectin type III domain is analogous to the natural evolution of disulfide bonds found in new antigen receptors of cartilaginous fish and in camelid heavy chain variable domains (17). Therefore, it appears that the acquisition of conserved cystine linkages to enhance structural stability is the result of convergent evolution (16).

The presence of an interloop cystine in dromedary HCAb-derived VHHs or platypus VH domains has been proposed to restrict the conformational flexibility of the long CDR3 loop in the antigen-free form and therefore to play an important role in reducing the paratope flexibility (18). Thus, the interloop cystine might affect the affinity by minimizing the entropic loss during loop fixation upon antigen complexation (19, 20). However, the significance of the interloop disulfide bond in antigen binding was never formally tested and is even questioned in some cases by the observation that multiple intracellularly expressed VHHs with Cys in their CDR loops are functional in the reducing environment of the cytoplasm (21–23) where disulfide bonds are supposedly not formed. To investigate the functional role of the interloop disulfide bond (*i.e.* its effect on affinity, stability, and the reaction pathway of antigen-antibody binding), we randomized the Cys residues forming the additional cystine in several well characterized VHHs. We chose VHHs with Cys at different locations within the loops and with different CDR3 lengths. This approach is preferred as the alternative strategy, the introduction of a new disulfide bond in a VHH without an interloop disulfide bond, might cause adverse effects (the replacement of other stability-enhancing effects, side chain restructuring, etc.).

Two different selection strategies (phage display and bacterial two hybrid (B2H)) were used to identify the functional antigen-specific variants without an interloop cystine, and the selected variants were studied in detail. Our results reveal the importance of the interloop disulfide bond in the stabilization of the VHH and in the affinity for the antigen.

EXPERIMENTAL PROCEDURES

Generation of Codon-randomized Libraries and Selection of Antigen-specific Variants—The Cys codons in the CDR1 and CDR3 of cAbAn33, cAbPSA-N7, cAbLys3, BM_GFP2, and BM_GFP3 were randomized by PCR with degenerate primers containing an "NNN" sequence to replace the "TGY." Libraries comprising the whole randomized repertoire were generated in the vector pHEN4 (24) or pBTL (*i.e.* a pBT vector from Stratagene that was modified to accommodate a VHH in its multiple cloning site) for *in vitro* panning or *in vivo* B2H selection, respectively. The final PCR fragments were ligated into the pHEN4 or pBTL vector after restriction with the enzymes NcoI/NotI or PstI/EcoRI, respectively. Ligated material was transformed in freshly prepared *Escherichia coli* TG1 or BMII cells (Stratagene) and plated on LB plates with ampicillin or chloramphenicol for subsequent phage display or bacterial two-hybrid selections, respectively. The colonies were scraped from the plates, washed, and stored in LB medium supplemented with glycerol (25% final concentration) at −80 °C.

The *in vitro* selection, *i.e.* panning, of the cAbAn33, cAbPSA-N7, and cAbLys3 TGY codon-randomized libraries on the trypanosome variant surface glycoprotein, human PSA, and hen egg white lysozyme (HEWL) antigens, respectively, were conducted under conditions similar to those for the selection of the parental VHHs (24–26). After panning, individual colonies were picked, and periplasmic expression of soluble VHH was carried out according to Saerens *et al.* (27). The periplasmic extract was tested in a solid-phase ELISA for antigen recognition. Maxisorb 96-well plates (Nunc) were coated overnight at 4 °C with antigen at 1 μg/ml in phosphate-buffered saline (PBS). Residual protein binding sites in the wells were blocked with 1% milk powder in PBS for 2 h at room temperature. After adding the VHH to the wells coated with its cognate antigen, the captured VHHs were detected with a mouse anti-hemagglutinin decapeptide tag (Berkeley Antibody Co.) followed by an anti-mouse conjugate (Sigma). The absorption at 405 nm was measured 15–30 min after adding the enzyme substrate *p*-nitrophenyl phosphate or 2,2′-azino-bis(3-ethylbenzathiazoline-6-sulfonic acid) for phosphatase or peroxidase conjugates, respectively. The *VHH* genes of the clones scoring positive in the solid-phase ELISA were sequenced, and different variants were chosen for further characterization.

B2H selections with BM_GFP2 and BM_GFP3 were performed according to instructions of the supplier of the plasmids and reporter cells (Stratagene). Plasmids pBT (encoding the full-length bacteriophage λ repressor protein) and pTRG (encoding the amino-terminal domain of the α-subunit of RNA polymerase) were purchased from Stratagene. A linker was introduced into the pBT, resulting in the pBTL vector. The cDNA of GFP (28), amplified by PCR to contain appropriate restriction enzyme sites, was cloned into the pTRG vector (29) between NotI and EcoRI sites. After confirming the proper sequence of the pTRG-GFP cDNA insert, plasmid DNA was prepared using a Qiagen miniprep kit. For bacterial two-hybrid experiments using the TGY codon-randomized libraries, a total

of 600 ng of pTRG-GFP was transformed in electrocompetent *E. coli* BMII cells (Stratagene) harboring the pBTL-VHH library, transforming aliquots of 75 ng of DNA into 75 μl of electrocompetent cells. All transformations were pooled in a single tube and incubated (1 h) in $M9^+$ His dropout minimal medium and Super Optimal broth with catabolite repression medium before aliquots were diluted from 10^{-1} to 10^{-6} and plated on various plates to calculate the transformation efficiency. The remaining cells were plated on large plates with single selective medium and allowed to grow for 24 h at 37 °C. Colonies were manually transferred to double selective medium plates and to LB-agar plates containing chloramphenicol (25 μg/ml). After 24-h incubation at 37 °C, surviving colonies on these plates were counted. The colonies on LB-agar plates containing chloramphenicol were used for the amplification of the *VHH* gene by PCR using pBT-Forw and pBT-Rev primers (Stratagene). After sequencing the *VHH* gene, different variants were chosen for further characterization.Variants for cAbAn33 C37*X*/C108*Y*, cAbPSA-N7 C38*X*/C111*Y*, cAbLys3 C38*X*/C111.6*Y*, BM_GFP2 C38*X*/C112.5*Y*, and BM_GFP3 C38*X*/C111.3*Y* are denoted as cAbAn33 *XY*, cAbPSA-N7 *XY*, cAbLys3 *XY*, BM_GFP2 *XY*, and BM_GFP3 *XY*, respectively, with *X* and *Y* denoting the Cys-substituted amino acid by its single letter code.

Expression and Purification of Antigen-specific VHH Variants—The genes of the variants that scored positive in ELISA after panning or B2H were recloned from pHEN4 or pBTL vector into the expression vector pHEN6 (30) using the restriction enzymes NcoI or PstI and BstEII, respectively. The plasmid constructs were transformed into *E. coli* WK6 (su−) cells. Expression in the periplasm and purification of recombinant VHH were carried out as described previously (30).

Surface Plasmon Resonance Measurements—The kinetic parameters of the wild type and variants were determined by surface plasmon resonance on Biacore 3000 and T100 instruments (GE Healthcare). For cAbPSA-N7 and BM_GFP2/3, different human PSA and GFP concentrations between 1 μM and 3 nM were added to the purified His_6-tagged VHH coated on a nickel-nitrilotriacetic acid biochip, respectively (25, 31). In case of cAbAn33 and cAbLys3, the AnTat1.1 variant surface glycoprotein and HEWL were covalently bound onto a CM5 chip via amine coupling (32, 33). Subsequently, different VHH concentrations between 2 μM and 3 nM were added onto the coupled antigen. The kinetic rate constants k_{on} and k_{off} and the equilibrium dissociation constant K_D were determined with BIAevaluation software version 4.1 (GE Healthcare). The kinetic rate values of every VHH were plotted on a two-dimensional diagram so that data points located on the same diagonal line have identical K_D values, *i.e.* a rate plane with isoaffinity diagonals (RaPID) plot.

For the transition state thermodynamic analysis of BM_GFP2 binding kinetics, surface plasmon resonance measurements were performed at four different temperatures, *i.e.* 15, 20, 25, and 30 °C. In case of cAbLys3, the temperatures were set at 10, 15, 20, 25, 30, and 35 °C. The kinetic data were evaluated using BIAevaluation 4.1 and T100 evaluation wizards (GE Healthcare). At each temperature and for each analyte, the reference-subtracted sensorgram obtained without analyte was subtracted from those for non-zero analyte concentrations. The resulting curves were fitted to the Langmuir 1:1 interaction model with local RMAX. The affinity constant K_D and association and dissociation rate constants k_{on} and k_{off} were obtained and fitted to the linear forms of the van't Hoff and Eyring equations to obtain ΔH^0 and ΔS^0 (18).

Chemical and Thermal Stability—The GdmCl-induced and heat-induced unfolding of different VHHs was determined according to Dumoulin *et al.* (19). Fluorescence at a single wavelength and the center of spectral mass of the intrinsic fluorescence emission spectra were used as chemical unfolding parameters (34). The intrinsic fluorescence of the protein at 25 μg/ml in 50 mM sodium phosphate, pH 7.0 and variable concentration of GdmCl was monitored with the excitation wavelength at 280 nm, and emission spectra were recorded from 300 to 420 nm. Heat-induced unfolding was measured in a spectropolarimeter (Jasco J-715) at a wavelength of 205 nm using a protein concentration of 0.1–0.2 mg/ml in 50 mM phosphate, pH 7.0 and a 0.1-cm cell path length. The temperature was increased from 35 to 95 °C at a rate of 1 °C/min. Data were acquired with a reading frequency of $1/20\ s^{-1}$, a 1-s integration time, and a 2-nm bandwidth. Data analysis of both chemical and thermal unfolding experiments was performed according to Saerens *et al.* (34).

Structural Representation and Modeling—All protein structural representations were produced with the PyMOL software of DeLano Scientific. Structure coordinates can either be found in the Protein Data Bank (codes 1YC7 (32), 1MEL (35), 2I24 (36), and 1SQ2 (37)) or were generated using the ESyPred3D web server (38) using their respective wild-type Protein Data Bank files as template. In addition, *ab initio* modeling for the wild type and mutants was performed using the Robetta server.

RESULTS

Replacing Amino Acids Forming Interloop Disulfide Bond within Different VHHs—Three different VHHs (cAbAn33, cAbLys3, and cAbPSA-N7) were chosen to randomize the Cys forming the interloop disulfide bond and to retrieve functional variants by *in vitro* selection, *i.e.* phage display. The cAbAn33, which has specificity for variant surface glycoprotein of trypanosomes (26, 39), has a short CDR3 of 12 amino acids that does not cover the FR-2 as is often seen for VHH (32) and harbors extra Cys residues in CDR1 and CDR3 at positions 37 and 108, respectively (Fig. 1). The cAbPSA-N7, which serves as capturing agent for human PSA (25) in biosensors, has a CDR3 of 14 amino acids and extra Cys residues in CDR1 and CDR3 at positions 38 and 111, respectively. The cAbLys3, which inhibits HEWL activity (40), has a very long CDR3 of 26 amino acid residues in part folding back over the FR-2 (35) and extra Cys residues in CDR1 and CDR3 at positions 38 and 111.6, respectively. This set of VHHs covers a broad range of CDR3 loop lengths, various locations of Cys in CDR1/CDR3 (Fig. 1), different loop structures (32, 41), and a variety of thermal and chemical stabilities (31, 34). Randomization of the extra Cys residues in cAbAn33, cAbPSA-N7, and cAbLys3 was performed by substituting the TGY codons with NNN. Libraries of VHH with randomized Cys codons were prepared for each VHH in the pHEN4 phage display vector with a size of 10^6 individual trans-

```
                1       10        20        30        40        50        60
                |       |         |         |         |         |         |
                <------- FR1-IMGT ------> <CDR1-IMGT > <--- FR2-IMGT --> <CDR2IMGT>
cAbBCII10       QVQLVESGG.GSVQAGGLRLSCTAS GGSEYS.YSTFS LGWFRQAPGQEREAVAA IASM  GGLT
cAbAn33         DVQLVESGG.GSVQAGGLRLSCAVS GSTY....SPCT TGWYRQAPGKEREWVSS ISSP...GTI
cAbPSA-N7       DVQLQESGG.GSVQAGGLRLSCVAS GWIY....IPPC MAWFRQAPGKERERVAT INPS...GRT
cAbLys3         DVQLQESGG.GSVQAGGLRLSCAAS GYTI....GPYC MGWFRQAPGKEREGVAA INMG..GGIT
BM_GFP2         DVQLQESGG.GSVQAGGLRLSCAAS PYFS....LRSC VAWFRQAPGKEREGVAT IFTS..TGST
BM_GFP3         DVQLQESGG.GSVQAGGLRLSCAAS GFPF....SNYC MGWFRQAPGKEREGVAT ISRL..GMFT

                   70        80        90       100       110                   120
                    |         |         |         |         | 1 3 5 7 5 3 1       |
                   <-------------FR3-IMGT ---------------> <------- CDR3-IMGT ------> <FR4-IMGT >
cAbBCII10       YYADSVK.GRFTISRDNAKNTVTLQMNNLKPEDTAIYYC AAVRGYFMR........LPSSHNFRY WGQGTQVTVSS
cAbAn33         YYDQSVK.GRFTISRDNAKNTVYLQMNSLQREDTGMYYC QIQCGV..............RSIREY WGQGTQVTVSS
cAbPSA-N7       YYADSTK.GRFTISQDNVKRTLYLYMNSLKPEDTATYYC AADDGTC.............PRMEFDD WGQGTQVTVSS
cAbLys3         YYADSVK.GRFTISQDNAKNTVYLLMNSLEPEDTAIYYC AADSTIYASYYECGHGLSTGGYVYDS WGQGTQVTVSS
BM_GFP2         YYADSVK.GRFTISQDNA.NTVSLQMNSLEPEDAAMYYC AIEGRPMIGGPS...CSMGSPNSYTY WGQGTQVTVSS
BM_GFP3         EYADSVQ.GRFIISRDNAQNMVFLQMNNLTPEDTAIYYC AAVSTSSSDCR.....PRLPSQEYTY WGQGTQVTVSS
```

FIGURE 1. **Alignment of VHH amino acid sequences to universal VHH scaffold cAbBCII10 (31).** The FRs, antigen-binding loops, CDRs, and amino acid numbering are according to IMGT. The hallmark amino acids in FR-2 that differentiate a VHH from VH are represented in *bold* and on a *gray background*. These VHH hallmark amino acids ((F/Y)ER(A/R/G)) are in VH highly conserved, hydrophobic (VGLW), and interact with the VL partner domain. The cysteines forming the VHH-characteristic interloop disulfide bond are highlighted in *white lettering* on a *black background*.

formants of which more than 75% contained a phasmid with a correctly sized insert.

In addition, two different VHHs, BM_GFP2 and BM_GFP3, were chosen to randomize the Cys participating in the interloop disulfide bond and for subsequent *in vivo* selection, *i.e.* a B2H selection, to retrieve functional variants. The BM_GFP2 and BM_GFP3 were selected previously by a B2H against GFP (42). Both binders have an additional Cys residue in CDR1 at position 38 and another Cys residue in CDR3 at positions 112.5 and 111.3 for BM_GFP2 and BM_GFP3, respectively. Their CDR3 lengths are 23 and 21 residues, respectively (Fig. 1). Randomization of the extra Cys residues in BM_GFP2 and BM_GFP3 was performed by replacing the TGY codon with NNN codons. The Cys-randomized libraries of BM_GFP2 and BM_GFP3 in pBTL had sizes of 10^8 and 1.2×10^8 individual transformants with 75 and 67% correctly sized inserts, respectively.

Selection of Variants by Phage Display and Bacterial Two Hybrid—The libraries of VHHs (in pHEN4) with the Cys of the loop randomized were subjected to three rounds of panning on immobilized antigens, *i.e.* variant surface glycoprotein, human PSA, and HEWL for cAbAn33, cAbPSA-N7, and cAbLys3, respectively. The experimental panning conditions for each library were similar to those in previous reports (24–26). Clear enrichment of virions with antigen-specific VHH was observed for each library at the third round of panning. For each selection, 48 colonies were picked randomly and cultured, and each periplasmic extract was screened for antigen binding. The *VHH* genes of the clones producing VHHs that scored positive in solid-phase ELISA were sequenced and recloned into the pHEN6 expression vector to allow large scale production of its soluble VHH variant.

The VHH libraries with randomized Cys cloned in the pBTL vector were subjected to B2H selection. In this screening procedure, colonies grow only on the plates with selective medium if an interaction occurs between a VHH variant and the antigen inside the cell. From each B2H screening, 64 colonies growing on double selective medium were picked randomly to sequence their *VHH* gene insert.

Sequence Variability in Functional Cys Variants—One, six, and seven different functional variants were isolated for cAbLys3, cAbPSA-N7, and cAbAn33, respectively. The Cys-37 of cAbAn33 was replaced by Ser, Phe, Arg, Asn, and Ile, whereas the Cys-108 was replaced by Met, Glu, and Phe. In the case of cAbPSA-N7, the Cys-38 was replaced by Thr, Arg, and Ser, whereas the Cys-111 was substituted by Gly, His, Glu, Ala, and Pro. For cAbLys3, only one functional variant could be isolated with C38S and C111.6P substitutions.

Among all functional cAbAn33 and cAbPSA-N7 variants, only one common substitution was found in both cases, *i.e.* the Arg-Glu variant. In the cAbAn33 variants, Phe and Met amino acid substitutions are overrepresented, whereas in cAbPSA-N7, the Thr and Gly replacements occur repeatedly. In the large CDR3 loop of cAbPSA-N7 and cAbLys3, Cys to Pro substitutions were observed.

As for the B2H selection, 17 and 42 different variants (of two groups of 64 colonies sent for sequencing) were identified for the BM_GFP2 and BM_GFP3, respectively. The Phe-Gly variant of BM_GFP2 was retrieved four times, whereas the Val-Pro and the Gly-Ser, His-Pro, Pro-Pro, Ser-Pro, Val-Gly, Val-Pro variants of BM_GFP3 were observed three and two times, respectively. Two BM_GFP2 variants had unpaired Cys residues in CDR1 and CDR3. Furthermore, there was a preference for Phe to substitute for the CDR1 Cys, whereas there was more freedom to replace the CDR3 Cys residue in BM_GFP2. In contrast, there was a preference for charged and, to a lesser extent, hydrophobic amino acids to substitute for the Cys in the CDR1 and CDR3 of BM_GFP3. In addition, Cys to Pro substitutions were favored in the CDR3 of BM_GFP3, and this was also apparent in cAbPSA-N7 and cAbLys3 mutants. From the available variants of BM_GFP2 and BM_GFP3, four and seven different variants were chosen for further characterization, respectively.

Expression and Purification of Parental and Functional Cys Variants—The selected variants were recloned from pHEN4 or pBTL into pHEN6 and expressed as soluble proteins in the periplasm of *E. coli* WK6. All variants of cAbAn33 and cAbLys3 were expressed at levels similar to the parental clones. Surprisingly, the cAbPSA-N7 variants revealed at least a 20-fold increase in expression compared with the original clone, pointing to possible difficulties of *E. coli* to express and fold the cAbPSA-N7 with an interloop disulfide bond. The expression yield of the B2H-selected variants was similar to the original BM_GFP2 and BM_GFP3 except for BM_GFP2 EL for which an increased yield was obtained. All variants folded in monomeric entities as their size exclusion chromatograph on Superdex 75 showed a single symmetrical peak eluting at the same volume of the parental-type VHH. It therefore seems that all these Cys substitutions are well tolerated in these VHHs.

Effects of Cys Substitutions on VHH Structure—To understand the impact of the structural changes upon deletion of the interloop disulfide bond, the three-dimensional structure of the mutants of cAbAn33 and cAbLys3 (for which the crystal structure is known) was modeled using the ESyPred3D server (38) and the Robetta server (see "Experimental Procedures"). In our experience, the ESyPred3D algorithm is more reliable compared with Phyre in predicting the correct three-dimensional structure of a VHH, and the models corresponded perfectly well to the models calculated by the Robetta server (data not shown). Modeling was performed for the cAbAn33 FE and RE mutants and for the cAbLys3 SP mutant (Fig. 2). Overall, the structural difference between the parental VHH and its Cys-substituted models is minimal. Remarkably, in the cAbAn33 variants, the side chains of the residues replacing the Cys (Phe, Arg, and Glu) stick outward, although the Cα–Cβ bonds of all mutants overlap with that of Cys (Fig. 2*A*). Evidently, the sulfhydryl groups of CDR1 and CDR3 Cys in cAbAn33 are directed toward each other to form the disulfide bond. Flipping out of the Phe, Arg, or Glu side chains occurs without rearranging the orientation of the adjacent (surrounding) amino acids. However, more distantly located amino acid side chains of Lys-84, Arg-112, and Arg-115 also changed their orientation in the Cys mutants (Fig. 2*A*).

For the cAbLys3 SP mutant, minor changes in the side chain orientation of adjacent residues Gln-3, Lys-84, and Glu-111.5 are noted. Because the Protein Data Bank file contains the coordinates of both the VHH and the HEWL antigen, we can infer directly the possible effect of the mutagenesis on antigen binding. Examination of the complex indicates that the side-chain reorganization of Glu-111.5 alters directly the interaction surface between antigen and VHH (Fig. 2*B*).

Effects of Cys Substitutions on Antigen Binding—The k_{on}, k_{off}, and K_D parameters were measured by surface plasmon resonance for every variant and are represented in a RaPID plot (Fig. 3). Compared with the original cAbAn33 with an equilibrium dissociation constant of 58 nM for its antigen, the variants show a 2–20-fold increase in K_D value. The cAbAn33 SF and RE variants are the best binders, whereas the cAbAn33 IM variant is the worst in antigen binding (Table 1). Upon inspection of the whole set of variants of cAbAn33, a modest increase in k_{on} values (2– 8-fold) is observed except in the case of the cAbAn33

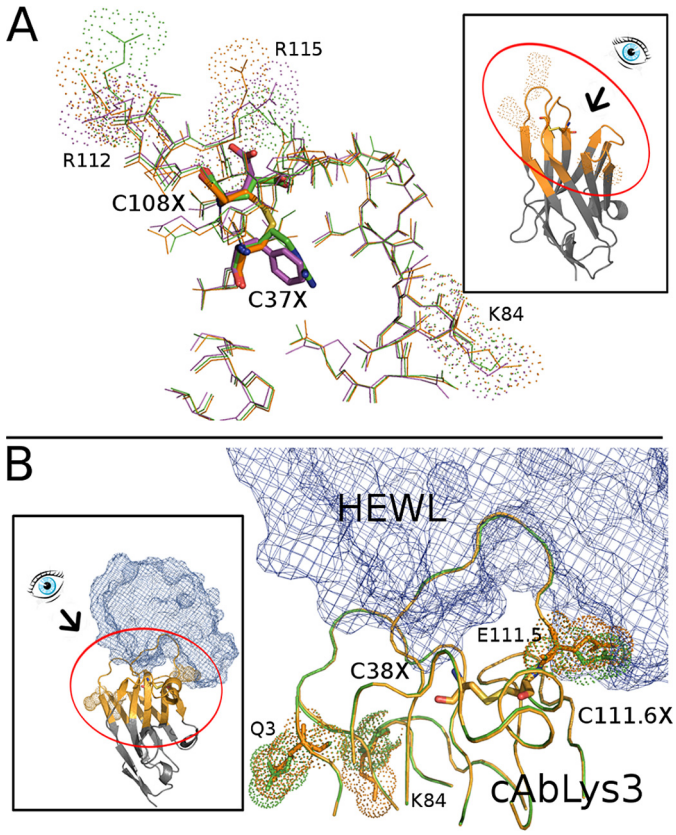

FIGURE 2. **Structural model of cAbAbn33 and cAbLys3.** *A*, *thin line stick* representation of the amino acid residues near the paratope of cAbAn33 (Protein Data Bank code 1YC7) (*orange*) superposed with two of the selected variants (cAbAn33 RE, *green*; cAbAn33 FE, *purple*). The interloop disulfide bond and the Cys-substituting residues are shown in *thicker line stick* representation colored by element, keeping the colors of the other amino acids of the VHH for the carbon atoms. The amino acids in the vicinity of cystine or its substitutions that differ in orientation are labeled and indicated by their surface contours. *B*, line presentation of cAbLys3 paratope (Protein Data Bank code 1MEL; *orange*) superposed on the cAbLys3 SP variant (*green*). The amino acids in the vicinity of cystine (Cys-38 and Cys-111.6) or its Ser-Pro substitutions that differ in orientation are labeled *Q3*, *K84*, and *E111.5*) and indicated by their surface contours. The interaction with the HEWL antigen (*blue chicken wire* representation) is also shown. Three-dimensional models of the WT and Cys mutant VHHs were generated using the ESyPred3D web server (38). *Insets* show the intact molecule and the eye view angle of the main picture.

FE variant (~27-fold decrease) (Fig. 3). In addition, the variants reveal an increase in k_{off} value by a factor of 6–20 except the cAbAn33 FE variant, which has a 4-fold decrease in k_{off}. Thus, the presence of the interloop disulfide bond of cAbAn33 has, on average, a beneficial effect on the k_{off}, compensating for the slightly lower k_{on} value.

In the case of the cAbPSA-N7 interaction with human PSA, the K_D value is 20–115-fold better than that of the selected mutants (Table 2). This significant drop in affinity for the cAbPSA-N7 variants originates from a 5-fold decrease in k_{on} value and an additional increase of the k_{off} value by a factor between 3 and 28 (Fig. 3). Thus, the presence of the interloop disulfide bond between CDR1 and CDR3 in cAbPSA-N7 seems to influence both the k_{on} and k_{off} values in the direction of enhanced binding.

For the only lysozyme-binding cAbLys3 SP mutant, an increase in K_D value is observed from 16 to 152 nM (Table 3). This 10-fold drop in affinity is attributed to a 3-fold increase in k_{off} and a 3-fold decrease in k_{on} values (Fig. 3).

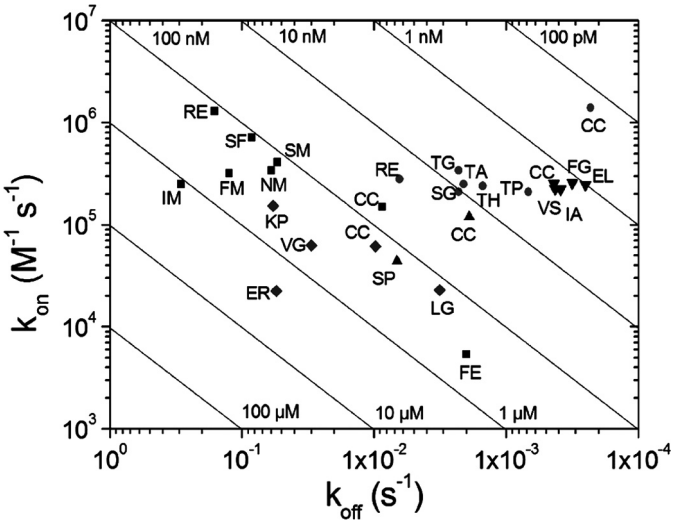

FIGURE 3. **RaPID plot for parental and variants of cAbAn33 (■), cAbPSA-N7 (●), cAbLys3 (▲), BM_GFP2 (▼), and BM_GFP3 (♦).** The single letter code for the interloop disulfide bonded Cys or its amino acid substitutions are given for each VHH.

TABLE 1

Melting temperature (T_m in °C), free energy of chemical unfolding (ΔG^0 in kJ mol^{-1}), m-value (kJ mol^{-1} M^{-1}), chemical denaturation midpoint (C_m in M), and equilibrium dissociation constant (K_D in nM) of different variants of cAbAn33

cAbAn33	T_m	ΔG^0	*m*-value	C_m	K_D
	°C	kJ mol^{-1}	kJ mol^{-1} M^{-1}	M	nM
Cys-Cys	71	34.2 ± 2.5	16.9 ± 2.1	2.10 ± 0.10	58
Ser-Met	61	24.2 ± 1.3	17.3 ± 1.3	1.40 ± 0.10	132
Ser-Phe	60	20.0 ± 2.0	14.5 ± 1.3	1.38 ± 0.10	117
Phe-Met	61	25.2 ± 1.5	16.5 ± 1.2	1.54 ± 0.10	391
Phe-Glu	59	19.8 ± 1.2	16.5 ± 0.8	1.20 ± 0.11	370
Ile-Met	62	24.7 ± 1.9	16.1 ± 1.2	1.53 ± 0.10	1160
Arg-Glu	57	14.6 ± 1.8	14.5 ± 1.3	1.00 ± 0.13	124
Asn-Met	60	15.3 ± 1.3	11.9 ± 1.0	1.28 ± 0.10	176

TABLE 2

Melting temperature (T_m in °C), free energy of chemical unfolding (ΔG^0 in kJ mol^{-1}), m-value (kJ mol^{-1} M^{-1}), chemical denaturation midpoint (C_m in M), and equilibrium dissociation constant (K_D in nM) of different variants of cAbPSA-N7

ND, not determined.

cAbPSA-N7	T_m	ΔG^0	*m*-value	C_m	K_D
	°C	kJ mol^{-1}	kJ mol^{-1} M^{-1}	M	nM
Cys-Cys	61	15.6 ± 1.0	11.4 ± 0.8	1.40 ± 0.05	0.2
Thr-His	53	ND	ND	ND	6.3
Thr-Ala	53	21.4 ± 1.5	16.8 ± 4.0	1.27 ± 0.10	8.4
Thr-Pro	57	19.4 ± 1.1	15.0 ± 2.9	1.29 ± 0.10	3.2
Thr-Gly	53	18.9 ± 0.7	16.2 ± 1.9	1.17 ± 0.10	6.8
Arg-Glu	51	19.9 ± 1.3	16.5 ± 2.9	1.20 ± 0.10	22.9
Ser-Gly	53	17.7 ± 1.2	17.0 ± 3.7	1.04 ± 0.10	11.0

TABLE 3

Melting temperature (T_m in °C), free energy of chemical unfolding (ΔG^0 in kJ mol^{-1}), m-value (kJ mol^{-1} M^{-1}), chemical denaturation midpoint (C_m in M), and equilibrium dissociation constant (K_D in nM) of different variants of cAbLys3

cAbLys3	T_m	ΔG^0	*m*-value	C_m	K_D
	°C	kJ mol^{-1}	kJ mol^{-1} M^{-1}	M	nM
Cys-Cys	69	27.1 ± 3.0	12.9 ± 1.3	2.04 ± 0.10	16
Ser-Pro	59	21.8 ± 1.6	11.5 ± 1.7	1.89 ± 0.05	152

In sharp contrast, the interloop disulfide bond does not give any improvement in antigen binding for BM_GFP2 (Fig. 3). The variants of BM_GFP2 reveal kinetic antigen binding parameters that are very similar to the parental type. Likewise, all selected variants of BM_GFP3 exhibit a similar K_D value (except the BM_GFP3 ER mutant); however, significant variations in either the k_{on} (*e.g.* larger k_{on} value for BM_GFP3 VP) and/or k_{off} value (*e.g.* BM_GFP3 LG) are noted relative to the original clone.

Effects on Transition State Thermodynamics of Binding—The temperature dependence of the antigen binding kinetics was monitored for cAbLys3, BM_GFP2, and their variants. The cAbLys3 interaction with HEWL has a gradually increasing association rate (larger k_{on}) and a faster dissociation rate (larger k_{off}) with increasing temperatures from 10 to 35 °C. As a result, the cAbLys3 binds slightly better as temperature increases, whereas the equilibrium dissociation constant of the cAbLys3 SP variant indicates a slightly reduced affinity at higher temperatures (Fig. 4*A*). The free energy profiles reveal similar activation free energies for both variants (Fig. 4*B*). However, there is a larger enthalpic penalty for the transition state formation of the cAbLys3 complex with HEWL compared with that of the cAbLys3 SP variant (Fig. 4*C*). This unfavorable enthalpic barrier is compensated by a favorable entropic contribution for the transition state formation with cAbLys3, whereas the entropic contribution in antigen binding is decreased in the cAbLys3 SP mutant (Fig. 4*D*).

In a similar temperature dependence study of the BM_GFP2 interaction with GFP, it was shown that the kinetic binding parameters of each variant follow closely the parameters of the parental VHH. That is, a faster k_{on} rate and faster k_{off} rate are noticed with increasing temperature. Likewise, the free energy profiles overlap nicely (Fig. 5*A*). However, the enthalpy and entropy contributions show diversion between the parental Cys-Cys and its variants (Fig. 5, *B* and *C*). Each less favorable enthalpic barrier is counteracted by more favorable entropic contribution and vice versa, resulting in equivalent free energy profiles.

Effects on Thermal and Chemical Stability of VHH Variants—The thermal stability, which was assessed by the melting temperature (T_m) value, for original VHHs and their variants was followed by circular dichroism measurements. Compared with the original cAbAn33, each of the variants has a significantly lower thermal stability (Fig. 6*A*). The T_m values range from 57 to 62 °C for the cAbAn33 RE and IM variants, respectively, with a mean ΔT_m between variants and the original cAbAn33 of 11 °C (Table 1). In the case of cAbPSA-N7, the thermal stability of the variants is decreased in a manner similar to that of the cAbAn33 variants (supplemental Fig. S1A). Excluding the cAbPSA-N7 TP variant that has only a 4 °C lower T_m, the mean ΔT_m between variants and parental cAbPSA-N7 is 8.2 °C (Table 2). The cAbLys3 SP variant has a ΔT_m of 10 °C compared with the original clone (Table 3 and supplemental Fig. S1B). These values were expected because the stability contribution of a native disulfide bond is 10 °C on average (5). Therefore, the interloop disulfide bond seems to contribute significantly to the stability of these VHHs. For the variants of the BM_GFP2 and BM_GFP3, the melting temperatures are on average 10.8 and 7.2 °C lower, respectively, than the values for the parental VHH (Tables 4 and 5 and supplemental Fig. S1, C and D).

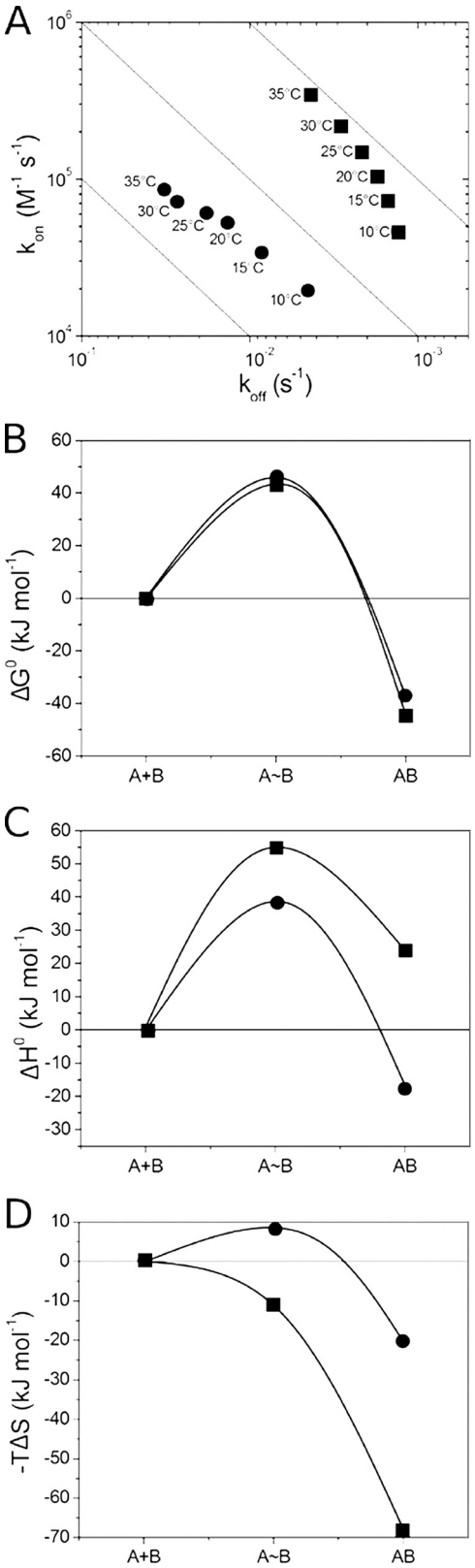

FIGURE 4. **Thermodynamic characterization of interaction between cAbLys3 CC (■) or cAbLys3 SP (ˆ) and HEWL.** *A*, RaPID plot of the VHH-HEWL interaction at six different temperatures between 10 and 35 °C (temperature indicated adjacent to each data point in the plot). *B–D*, the reaction pathway of cAbLys3 CC or cAbLys3 SP interaction with HEWL. The changes in ΔG^0, ΔH^0, and $-T\Delta S$ (*B*, *C*, and *D*, respectively) along the reaction coordinate are given for the initial unassociated state ($A+B$), the transition state ($A\sim B$), and the antibody-antigen complex (*AB*).

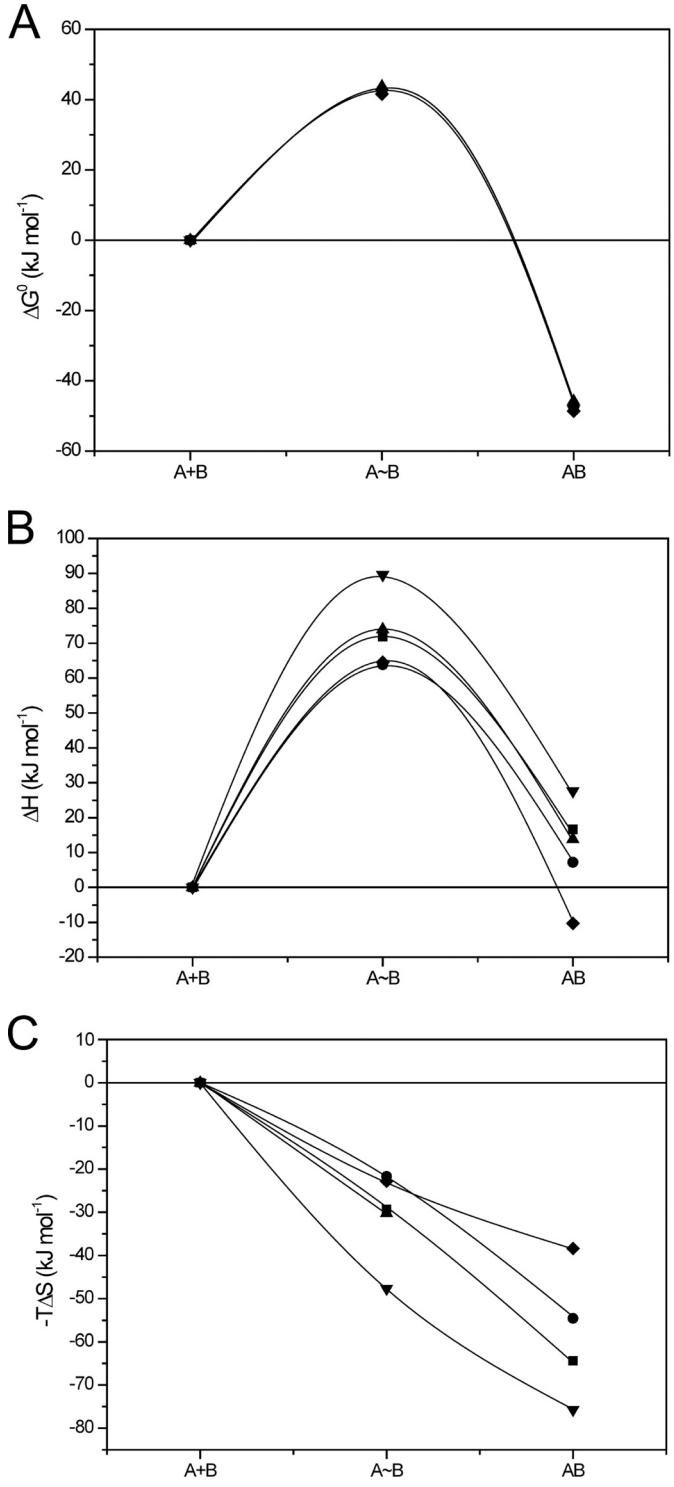

FIGURE 5. **Thermodynamic characterization of interaction between BM_GFP2 (CC (■), FG (●), IA (▲), EL (▼), or VS (♦)) and GFP along reaction pathway.** The changes in ΔG^0, ΔH^0, and $-T\Delta S$ (*A*, *B*, and *C*, respectively) along the reaction coordinate are given for the initial unassociated state ($A+B$), the transition state ($A\sim B$), and the antibody-antigen complex (*AB*).

In addition to the thermal stability, the GdmCl-induced unfolding of the phage display-selected variants was followed by their intrinsic fluorescence. The free energies of unfolding and the midpoint of chemical denaturation for the cAbAn33 variants (Fig. 6*B*) dropped on average 13.7 kJ/mol and 0.77 M, respectively (Table 1). The cAbAn33 RE variant, possibly form-

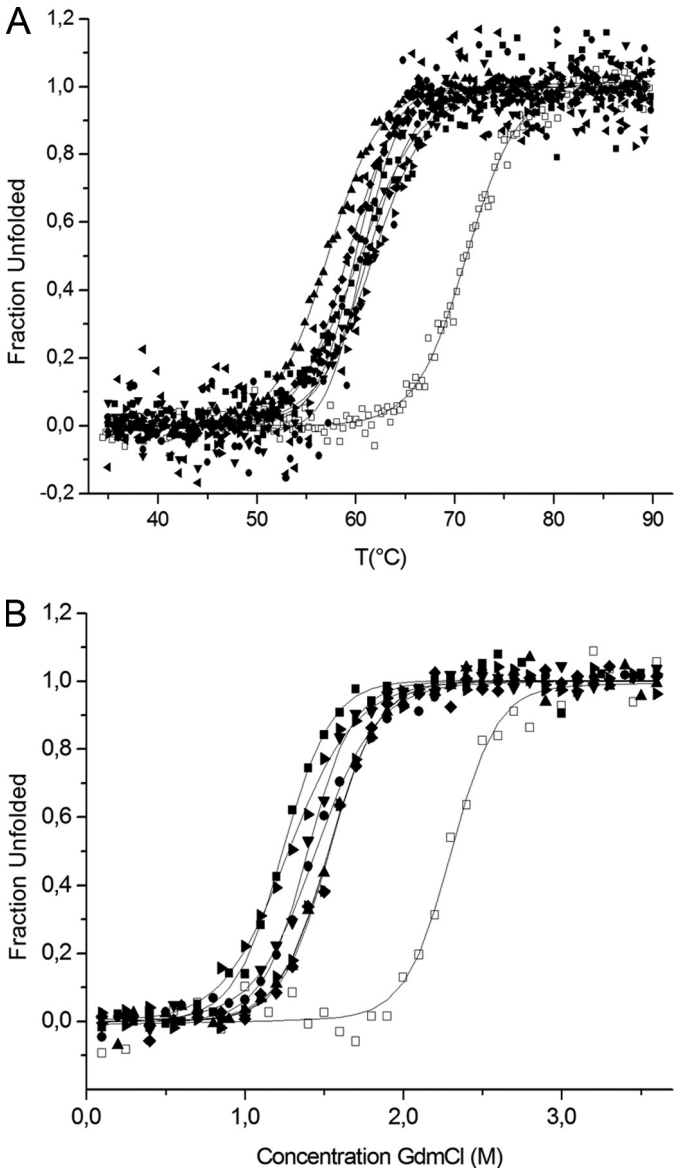

FIGURE 6. **Fraction of unfolded cAbAn33 as function of temperature (*A*) or GdmCl concentration (*B*).** Properly folded VHH at 35 °C or in a physiological buffer is unfolded by gradually increasing the temperature or the GdmCl concentration, respectively. The unfolding is followed spectrophotometrically, and the data are treated according to Saerens *et al.* (34). The *open symbols* in *A* and *B* (○ and □) are for the native cAbAn33 CC, and the *filled symbols* are for its variants (SM, ˆ; RE, ▲; FM, ▼; FE, ◆; SF, ◭; IM, ◮; NM, ■).

TABLE 4
Melting temperature (T_m in °C) and equilibrium dissociation constant (K_D in nM) of different variants of BM_GFP2

BM_GFP2	T_m	K_D
	°C	nM
Cys-Cys	78	1.7
Phe-Gly	67	1.2
Glu-Leu	63	1.0
Ile-Ala	69	1.7
Val-Ser	70	1.9

ing a hydrogen bond with the surrounding residues (Fig. 2), was the least stable cAbAn33 mutant with T_m, C_m, and ΔG^0 values of 57 °C, 1.00 M, and 14.6 kJ/mol, respectively. Regarding the chemical unfolding of cAbPSA-N7 variants, a large change in the *m*-value was measured for the variants compared with the parental protein (supplemental Fig. S1E). This might be attributed to a large change in accessible surface area upon unfolding (43), and it results in an overall decrease in C_m value by 0.21 M but an increase of free energy of unfolding of 3.9 kJ/mol (Table 2). The chemical stability for the cAbPSA-N7 TH variant could not be measured as the protein precipitated during the concentration step in the purification protocol. The cAbLys3 SP variant followed the trend of the cAbAn33 variants (supplemental Fig. S1F) with the free energy of unfolding and the midpoint of chemical denaturation dropping by 5.3 kJ/mol and 0.15 M, respectively (Table 3).

TABLE 5
Melting temperature (T_m in °C) and equilibrium dissociation constant (K_D in nM) of different variants of BM_GFP3

BM_GFP3	T_m	K_D
	°C	nM
Cys-Cys	78	158
Lys-Pro	71	379
Val-Pro	69	305
Lys-Arg	74	527
Glu-Arg	69	2436
Leu-Gly	70	139
Val-Gly	72	475

DISCUSSION

The role and importance of the distinctive FR-2 hallmark amino acids of VHHs are well established. The exact function of a less pronounced hallmark, *i.e.* the interloop disulfide bond in dromedary VHHs, has yet to be clarified. It was observed that dromedary-derived VHHs (and shark V-NAR (New Antigen Receptor) type II (15, 16)) frequently have an interloop disulfide bond connecting CDR1 and CDR3 (certainly those with a longer CDR3). In contrast, such disulfide tethers are rare or even absent in dromedary-derived VHs (from classic antibodies).

Because the same *D* and *J* germ line gene elements are used for both the *VHH-D-J* and *VH-D-J* rearrangements (12), the presence or absence of a Cys amino acid in the CDR3 of VHH or VH, respectively, is possibly caused by a differential selection. The introduction of a single Cys in the CDR3 during the *VH-D-J* rearrangement will probably lead to a counterselection of the B-cell expressing such a VH domain as there are no extra Cys residues encoded in the camelid *VH* germ line genes. For VHHs, however, the vast majority of the dromedary *VHH* germ line genes already encode a Cys in their CDR1 (13, 44). Therefore, the insertion of an extra Cys at the CDR3 will be favored as it allows the formation of an interloop disulfide bond. The Cys codon within the CDR3 might be encoded by the selected reading frame of the particular *D* gene that was used in the *VHH-D-J* recombination (45); it could be generated at the *VHH-D* or *D-J* junction (46), somatically introduced by random N nucleotide addition, or introduced subsequently by somatic hypermutation (47). The knock-in of a Cys in the CDR3 (certainly for VHHs with a longer CDR3) occurs much more frequently than a knock-out of the Cys in the CDR1. This suggests that the presence of an interloop cystine provides a selective advantage for the VHH domain. We propose that two driving forces are at the origin of the evolution and selection of VHHs with an interloop disulfide bond: (i) the reduction of the loss in entropy upon binding to the antigen and (ii) the overall stability of the folded VHH domain.

Effects of Cystine on Parameters of Antigen Binding—For most VHHs we tested, those mutants without an interloop disulfide bond have higher K_D values for binding to their cognate antigen than the wild-type VHHs with interloop cystines. Hence, during *in vivo* affinity maturation, the B-cell receptor with an interloop disulfide bond in its VHH will have a selective advantage over the variant lacking such a cystine. However, the difference in affinity is marginal for some Cys mutants. The BM_GFP2 variants, retrieved through B2H selection, have even a K_D value (1–2 nM) identical to that of the parental VHH. Likewise, the BM_GFP3 LG and VP and the cAbAn33 SF and RE have K_D values that are less than a factor 2 different from the cystine-containing VHH. The difference in HEWL affinity between cAbLys3 and the single cAbLys3 SP variant that was retrieved is 10-fold. Therefore, a major difference in affinity between the wild type and its variants without the interloop cystine is measured for cAbPSA-N7 (difference in affinity by at least a factor of 16 or more), but these mutants are better expressed compared with the parental VHH. So it may be that these variants are retrieved during phage display selection because of a facilitated expression rather than for their antigen affinity.

Surprisingly, multiple amino acid pairs are able to substitute for the interloop Cys and still generate an antigen-binding VHH. However, the number of antigen-specific VHH variants isolated after phage display is inversely proportional to their CDR3 length; *i.e.* a VHH with a shorter CDR3 yields more variants. This is exactly what is observed for the antigen-specific binders that are retrieved from immune dromedary VHH libraries as well: the VHHs with a longer CDR3 have a higher probability to contain an interloop disulfide bond.

The inverse correlation between CDR3 length and probability of occurrence of an interloop cystine is in line with the hypothesis that a longer CDR3 loop will have a larger conformational flexibility in the antigen-free form than shorter CDR3 loops. Therefore, the VHHs with a longer CDR3 loop will suffer more from the entropic loss upon binding to the antigen, and the presence of an interloop cystine will become more beneficial. Thus, removal of the interloop cystine bond in the VHHs with a longer CDR3 will result in a significant change in affinity or even a complete loss of binding caused by the adverse effect of the loss of entropy on the overall Gibbs free energy change of binding to the antigen.

The transition state thermodynamics of the binding kinetics corroborate this hypothesis. The antigen binding of wild-type VHHs with an interloop disulfide bond has a high enthalpic barrier that is counteracted by a favorable entropic contribution. The same observation was made for multiple affinity-matured antibody-antigen binding pairs (48). In addition, the dramatic change in thermodynamics of antigen binding upon elimination of the interloop cystine in the VHH illustrates the major role of this cystine by fixing the longer CDR3 loop into an optimal conformation and in reducing the entropic loss during antigen binding.

Stabilizing Effect of Interloop Cystine as Selective Feature of VHH—The second possible benefit from the presence of an interloop disulfide bond originates from its contribution to the intrinsic stability of the VHH domain. In a first study on the role of an interloop disulfide bond (49), an extra cystine was introduced into a human VH domain between residues 33 (CDR1) and 100b (CDR3) (Kabat numbering (50)). This mutation led to a slight increase in melting temperature ($\Delta T_m < 3$ °C). Remarkably, the additional randomization of amino acids surrounding the Cys-100b yielded antibody fragments with markedly increased melting temperatures ($\Delta T_m > 10$ °C). It seems that the introduction of two Cys residues forming an interloop disulfide bond is insufficient to profoundly stabilize a human VH domain. Additional amino acid mutagenesis is required to observe a marked increase in thermal stability of the VH antibody fragment.

In this study, we performed the opposite experiment and evaluated the stability of the domain after eliminating the interloop cystine. Although the chemical destabilization of the VHH domain by the cystine removal is obscured (at least for cAbLys3 and cAbPSA-N7) due to the changing *m*-value, which correlates to the differential accessible surface area upon unfolding (43), it is clear that the thermal stability of our VHHs decreases significantly (average ΔT_m of 9.2 °C). Therefore, it is obvious that the interloop disulfide bond contributes significantly to the intrinsic stability of the VHH. For VHH domains of low intrinsic stability, the absence of the interloop cystine might become detrimental to function as an autonomous VHH within an HCAb. Because the presence of the FR-2 hallmark amino acids in a VHH result in a net domain destabilization that cannot be compensated by the association of a stable VL partner, the evolution toward the presence of a stabilizing interloop disulfide bond constitutes an elegant solution.

REFERENCES

1. Williams, A. F., and Barclay, A. N. (1988) The immunoglobulin superfamily—domains for cell surface recognition. *Annu. Rev. Immunol.* **6,** 381–405
2. Lesk, A. M., and Chothia, C. (1982) Evolution of proteins formed by β-sheets. II. The core of the immunoglobulin domains. *J. Mol. Biol.* **160,** 325–342
3. Lefranc, M. P. (2004) IMGT-ONTOLOGY and IMGT databases, tools and web resources for immunogenetics and immunoinformatics. *Mol. Immunol.* **40,** 647–660
4. Abkevich, V. I., and Shakhnovich, E. I. (2000) What can disulfide bonds tell us about protein energetics, function and folding: simulations and bioinformatics analysis. *J. Mol. Biol.* **300,** 975–985
5. Betz, S. F. (1993) Disulfide bonds and the stability of globular proteins. *Protein Sci.* **2,** 1551–1558
6. Clarke, J., Hounslow, A. M., Bond, C. J., Fersht, A. R., and Daggett, V. (2000) The effects of disulfide bonds on the denatured state of barnase. *Protein Sci.* **9,** 2394–2404
7. Wedemeyer, W. J., Welker, E., Narayan, M., and Scheraga, H. A. (2000) Disulfide bonds and protein folding. *Biochemistry* **39,** 4207–4216
8. Welker, E., Wedemeyer, W. J., Narayan, M., and Scheraga, H. A. (2001) Coupling of conformational folding and disulfide-bond reactions in oxidative folding of proteins. *Biochemistry* **40,** 9059–9064
9. Tsai, C. H., Chan, C. H., Chen, B. J., Kao, C. Y., Liu, H. L., and Hsu, J. P. (2007) Bioinformatics approaches for disulfide connectivity prediction. *Curr. Protein Pept. Sci.* **8,** 243–260
10. Hamers-Casterman, C., Atarhouch, T., Muyldermans, S., Robinson, G., Hamers, C., Songa, E. B., Bendahman, N., and Hamers, R. (1993) Naturally occurring antibodies devoid of light chains. *Nature* **363,** 446–448
11. Saerens, D., Ghassabeh, G. H., and Muyldermans, S. (2008) Single-domain antibodies as building blocks for novel therapeutics. *Curr. Opin. Pharmacol.* **8,** 600–608
12. Conrath, K. E., Wernery, U., Muyldermans, S., and Nguyen, V. K. (2003) Emergence and evolution of functional heavy-chain antibodies in Cameli-

dae. *Dev. Comp. Immunol.* **27,** 87–103
13. Nguyen, V. K., Muyldermans, S., and Hamers, R. (1998) The specific variable domain of camel heavy-chain antibodies is encoded in the germline. *J. Mol. Biol.* **275,** 413–418
14. Johansson, J., Aveskogh, M., Munday, B., and Hellman, L. (2002) Heavy chain V region diversity in the duck-billed platypus (*Ornithorhynchus anatinus*): long and highly variable complementarity-determining region 3 compensates for limited germline diversity. *J. Immunol.* **168,** 5155–5162
15. Roux, K. H., Greenberg, A. S., Greene, L., Strelets, L., Avila, D., McKinney, E. C., and Flajnik, M. F. (1998) Structural analysis of the nurse shark (new) antigen receptor (NAR): molecular convergence of NAR and unusual mammalian immunoglobulins. *Proc. Natl. Acad. Sci. U.S.A.* **95,** 11804–11809
16. Nuttall, S. D., Irving, R. A., and Hudson, P. J. (2000) Immunoglobulin VH domains and beyond: design and selection of single-domain binding and targeting reagents. *Curr. Pharm. Biotechnol.* **1,** 253–263
17. Lipovsek, D., Lippow, S. M., Hackel, B. J., Gregson, M. W., Cheng, P., Kapila, A., and Wittrup, K. D. (2007) Evolution of an interloop disulfide bond in high-affinity antibody mimics based on fibronectin type III domain and selected by yeast surface display: molecular convergence with single-domain camelid and shark antibodies. *J. Mol. Biol.* **368,** 1024–1041
18. De Genst, E., Handelberg, F., Van Meirhaeghe, A., Vynck, S., Loris, R., Wyns, L., and Muyldermans, S. (2004) Chemical basis for the affinity maturation of a camel single domain antibody. *J. Biol. Chem.* **279,** 53593–53601
19. Dumoulin, M., Conrath, K., Van Meirhaeghe, A., Meersman, F., Heremans, K., Frenken, L. G., Muyldermans, S., Wyns, L., and Matagne, A. (2002) Single-domain antibody fragments with high conformational stability. *Protein Sci.* **11,** 500–515
20. Muyldermans, S., Atarhouch, T., Saldanha, J., Barbosa, J. A., and Hamers, R. (1994) Sequence and structure of VH domain from naturally occurring camel heavy chain immunoglobulins lacking light chains. *Protein Eng.* **7,** 1129–1135
21. Rothbauer, U., Zolghadr, K., Muyldermans, S., Schepers, A., Cardoso, M. C., and Leonhardt, H. (2008) A versatile nanotrap for biochemical and functional studies with fluorescent fusion proteins. *Mol. Cell. Proteomics* **7,** 282–289
22. Rothbauer, U., Zolghadr, K., Tillib, S., Nowak, D., Schermelleh, L., Gahl, A., Backmann, N., Conrath, K., Muyldermans, S., Cardoso, M. C., and Leonhardt, H. (2006) Targeting and tracing antigens in live cells with fluorescent nanobodies. *Nat. Methods* **3,** 887–889
23. Serruys, B., Van Houtte, F., Farhoudi-Moghadam, A., Leroux-Roels, G., and Vanlandschoot, P. (2010) Production, characterization and in vitro testing of HBcAg-specific VHH intrabodies. *J. Gen. Virol.* **91,** 643–652
24. Arbabi Ghahroudi, M., Desmyter, A., Wyns, L., Hamers, R., and Muyldermans, S. (1997) Selection and identification of single domain antibody fragments from camel heavy-chain antibodies. *FEBS Lett.* **414,** 521–526
25. Saerens, D., Kinne, J., Bosmans, E., Wernery, U., Muyldermans, S., and Conrath, K. (2004) Single domain antibodies derived from dromedary lymph node and peripheral blood lymphocytes sensing conformational variants of prostate-specific antigen. *J. Biol. Chem.* **279,** 51965–51972
26. Stijlemans, B., Conrath, K., Cortez-Retamozo, V., Van Xong, H., Wyns, L., Senter, P., Revets, H., De Baetselier, P., Muyldermans, S., and Magez, S. (2004) Efficient targeting of conserved cryptic epitopes of infectious agents by single domain antibodies. African trypanosomes as paradigm. *J. Biol. Chem.* **279,** 1256–1261
27. Saerens, D., Stijlemans, B., Baral, T. N., Nguyen Thi, G. T., Wernery, U., Magez, S., De Baetselier, P., Muyldermans, S., and Conrath, K. (2008) Parallel selection of multiple anti-infectome nanobodies without access to purified antigens. *J. Immunol. Methods* **329,** 138–150
28. Scholz, O., Thiel, A., Hillen, W., and Niederweis, M. (2000) Quantitative analysis of gene expression with an improved green fluorescent protein p6. *Eur. J. Biochem.* **267,** 1565–1570
29. Dove, S. L., Joung, J. K., and Hochschild, A. (1997) Activation of prokaryotic transcription through arbitrary protein-protein contacts. *Nature* **386,** 627–630
30. Conrath, K. E., Lauwereys, M., Galleni, M., Matagne, A., Frère, J. M., Kinne, J., Wyns, L., and Muyldermans, S. (2001) β-Lactamase inhibitors derived from single-domain antibody fragments elicited in the Camelidae. *Antimicrob. Agents Chemother.* **45,** 2807–2812
31. Saerens, D., Pellis, M., Loris, R., Pardon, E., Dumoulin, M., Matagne, A., Wyns, L., Muyldermans, S., and Conrath, K. (2005) Identification of a universal VHH framework to graft non-canonical antigen-binding loops of camel single-domain antibodies. *J. Mol. Biol.* **352,** 597–607
32. Conrath, K., Vincke, C., Stijlemans, B., Schymkowitz, J., Decanniere, K., Wyns, L., Muyldermans, S., and Loris, R. (2005) Antigen binding and solubility effects upon the veneering of a camel VHH in framework-2 to mimic a VH. *J. Mol. Biol.* **350,** 112–125
33. De Genst, E., Areskoug, D., Decanniere, K., Muyldermans, S., and Andersson, K. (2002) Kinetic and affinity predictions of a protein-protein interaction using multivariate experimental design. *J. Biol. Chem.* **277,** 29897–29907
34. Saerens, D., Conrath, K., Govaert, J., and Muyldermans, S. (2008) Disulfide bond introduction for general stabilization of immunoglobulin heavy-chain variable domains. *J. Mol. Biol.* **377,** 478–488
35. Desmyter, A., Transue, T. R., Ghahroudi, M. A., Thi, M. H., Poortmans, F., Hamers, R., Muyldermans, S., and Wyns, L. (1996) Crystal structure of a camel single-domain VH antibody fragment in complex with lysozyme. *Nat. Struct. Biol.* **3,** 803–811
36. Stanfield, R. L., Dooley, H., Verdino, P., Flajnik, M. F., and Wilson, I. A. (2007) Maturation of shark single-domain (IgNAR) antibodies: evidence for induced-fit binding. *J. Mol. Biol.* **367,** 358–372
37. Stanfield, R. L., Dooley, H., Flajnik, M. F., and Wilson, I. A. (2004) Crystal structure of a shark single-domain antibody V region in complex with lysozyme. *Science* **305,** 1770–1773
38. Lambert, C., Léonard, N., De Bolle, X., and Depiereux, E. (2002) ESyPred3D: Prediction of proteins 3D structures. *Bioinformatics* **18,** 1250–1256
39. Baral, T. N., Magez, S., Stijlemans, B., Conrath, K., Vanhollebeke, B., Pays, E., Muyldermans, S., and De Baetselier, P. (2006) Experimental therapy of African trypanosomiasis with a nanobody-conjugated human trypanolytic factor. *Nat. Med.* **12,** 580–584
40. Lauwereys, M., Arbabi Ghahroudi, M., Desmyter, A., Kinne, J., Hölzer, W., De Genst, E., Wyns, L., and Muyldermans, S. (1998) Potent enzyme inhibitors derived from dromedary heavy-chain antibodies. *EMBO J.* **17,** 3512–3520
41. Decanniere, K., Muyldermans, S., and Wyns, L. (2000) Canonical antigen-binding loop structures in immunoglobulins: more structures, more canonical classes? *J. Mol. Biol.* **300,** 83–91
42. Kirchhofer, A., Helma, J., Schmidthals, K., Frauer, C., Cui, S., Karcher, A., Pellis, M., Muyldermans, S., Casas-Delucchi, C. S., Cardoso, M. C., Leonhardt, H., Hopfner, K. P., and Rothbauer, U. (2010) Modulation of protein properties in living cells using nanobodies. *Nat. Struct. Mol. Biol.* **17,** 133–138
43. Myers, J. K., Pace, C. N., and Scholtz, J. M. (1995) Denaturant m values and heat capacity changes: relation to changes in accessible surface areas of protein unfolding. *Protein Sci.* **4,** 2138–2148
44. Nguyen, V. K., Hamers, R., Wyns, L., and Muyldermans, S. (2000) Camel heavy-chain antibodies: diverse germline V(H)H and specific mechanisms enlarge the antigen-binding repertoire. *EMBO J.* **19,** 921–930
45. Jones, J. M., and Gellert, M. (2004) The taming of a transposon: V(D)J recombination and the immune system. *Immunol. Rev.* **200,** 233–248
46. Furukawa, K., Akasako-Furukawa, A., Shirai, H., Nakamura, H., and Azuma, T. (1999) Junctional amino acids determine the maturation pathway of an antibody. *Immunity* **11,** 329–338
47. Li, Z., Woo, C. J., Iglesias-Ussel, M. D., Ronai, D., and Scharff, M. D. (2004) The generation of antibody diversity through somatic hypermutation and class switch recombination. *Gene Dev.* **18,** 1–11
48. Manivel, V., Sahoo, N. C., Salunke, D. M., and Rao, K. V. (2000) Maturation of an antibody response is governed by modulations in flexibility of the antigen-combining site. *Immunity* **13,** 611–620
49. Davies, J., and Riechmann, L. (1996) Single antibody domains as small recognition units: design and in vitro antigen selection of camelized, human VH domains with improved protein stability. *Protein Eng.* **9,** 531–537
50. Kabat, E. A., Wu, T. T., Perry, H. M., Gottesman, K. S., and Foeller, C. (1991) *Sequence of Proteins of Immunological Interest,* NIH Publication *Number* 91-3242, United States Department of Health and Human Services, Washington, DC